Laser-pulse photoassociation in a thermal gas of atoms

Emanuel F. de Lima,* Tak-San Ho,† and Herschel Rabitz‡
Department of Chemistry, Frick Laboratory, Princeton University, Princeton, New Jersey 08544, USA
(Received 11 July 2008; published 19 December 2008)

A nonperturbative treatment is presented for laser-pulse-driven formation of heteronuclear diatomic molecules in a thermal gas of atoms. Based on the assumption of full controllability, the maximum possible photoassociation yield is obtained. A one-dimensional model is used for calculating the photoassociation probability as a function of the laser parameters as well as for different temperatures. The dependence of the photoassociation yield on the laser frequency and amplitude reveals complex patterns of one- and multiphoton transitions. The photoassociation yield induced by subpicosecond pulses of *a priori* fixed shape is very low compared to the maximum possible yield.

DOI: 10.1103/PhysRevA.78.063417 PACS number(s): 34.50.Rk, 82.50.Nd, 32.80.Rm

I. INTRODUCTION

The formation of chemical bonds is one of the most fundamental processes in chemistry. In photoassociation, the binding of colliding atoms is facilitated by means of an external field, which induces a free-to-bound transition, forming a molecule in either the electronic excited or ground state. The identification of proper external fields opens up access to control of a variety of photoassociation processes [1].

Absorption and emission spectroscopy can provide insight into photoassociation [2–6] and femtosecond pulses have been applied to study photoassociation reactions [7–9]. The investigation of photoassociation processes is receiving increasing attention, mainly sparked by experimental developments with ultracold atomic and molecular gases [10–16]. Most of those investigations involve the absorption of visible or ultraviolet radiation by the colliding atoms to create a molecule in an electronically excited state. Subsequently, the formation of a molecule in its electronic ground state may be accomplished by either spontaneous or stimulated emission.

The photoassociation dynamics has also been studied with temperatures well above millikelvins in the thermal energy domain, which is a regime commonly encountered in the laboratory [9,17–21]. An alternative photoassociation mechanism can be envisioned based on the use of infrared pulses to drive a transition from free colliding atoms on the electronic ground state energy surface to form a molecule directly on that surface [17]. This approach requires the existence of non-negligible electric-dipole coupling between the free atomic states and the rovibrational levels of the ground electronic state of the molecule to be formed. This situation is often modeled as an atomic beam with a Gaussian wave packet describing the initial state of the colliding atomic pair [17–21].

In the present work, we investigate the photoassociation in a thermal gas of two different atomic species. The gas is assumed to be initially in translational thermal equilibrium while being subjected to an intense laser pulse, which aims to form a heteronuclear diatomic molecule. Assuming only binary collisions between the atoms and that the laser-induced transitions occur in the ground electronic state, we derive an expression for the photoassociation probability. Temperatures ranging over $1 \leqslant T \leqslant 500$ K are considered. Unlike previous investigations in the thermal regime based on this mechanism [17–21], here the total photoassociation probability is obtained by incoherently averaging the transitions from the Boltzmann-weighted scattering states. In performing atomic scattering calculations, it is often desirable to use square-integrable eigenstates as basis functions [22]. This can be achieved by considering the system confined to a suitable finite-size box [23,24]. Upon increasing the size of the box, the standing waves of the box will approximate the scattering states of the continuum. This paper considers a truncated Morse potential with an infinite barrier at long range to model the relative motion of a colliding atomic pair [25]. Moreover, based on considerations of control theory and assuming full controllability of the system [26–30] the maximum possible photoassociation yield are evaluated.

In Sec. II, a general formalism is presented for obtaining the photoassociation probability of a thermal atomic ensemble. A computationally practical model for colliding atomic pairs based on the Morse potential is presented and the upper bound of the photoassociation yield is determined. In Sec. III, the numerical results are presented for the photoassociation probability as a function of the pulse parameters and for several temperatures. Finally, conclusions are drawn in Sec. IV.

II. PHOTOASSOCIATION IN A THERMAL GAS OF ATOMS

Consider a dilute gas of atoms composed of two distinct atomic species at translational thermal equilibrium and subjected to an intense laser pulse. Assuming that only binary collisions take place, the goal is to determine the probability of forming heteronuclear diatomic molecules induced by the laser pulse. In the absence of the external field, the density operator of two colliding atoms in the gas is

*eflima@ifi.unicamp.br
†tsho@princeton.edu
‡hrabitz@princeton.edu

$$\hat{\rho}(t=0)=\frac{1}{Z}e^{-\beta\hat{H}_0}, \tag{1}$$

where $\hat{H}_0$ is the field-free Hamiltonian, $Z=\mathrm{Tr}\{e^{-\beta\hat{H}_0}\}$ is the partition function, and $\beta^{-1}=k_BT$ with k_B being the Boltzmann constant and T the temperature.

For simplicity, the field-free Hamiltonian $\hat{H}_0$ is taken to have a nondegenerate spectrum, consisting of discrete bound states $|\phi_\nu\rangle$ with energy E_ν and continuous scattering states $|\phi(E)\rangle$ with energy E. The gas at full thermal equilibrium will have some fraction of diatomic molecules present. The focus here before the laser pulse is on (a) the remaining unbound atoms or equivalently on (b) a nascent gas only consisting of atoms in translational equilibrium. Thus, before the laser field is turned on, the corresponding density operator can be written as an integral over the scattering states

$$\hat{\rho}(t=0)=\frac{1}{Z}\int_0^\infty e^{-\beta E}|\phi(E)\rangle\langle\phi(E)|dE. \tag{2}$$

The thermally averaged probability P_ν of the laser transferring the system into the bound state $|\phi_\nu\rangle$ at time t is

$$P_\nu(t)=\mathrm{Tr}[|\phi_\nu\rangle\langle\phi_\nu|\hat{U}(t,0)\hat{\rho}(t=0)\hat{U}^\dagger(t,0)], \tag{3}$$

where $\hat{U}(t,0)$ is the time-evolution operator satisfying the Schrödinger equation corresponding to the time-dependent Hamiltonian $\hat{H}=\hat{H}_0+\hat{H}_I(t)$, which includes the interaction of the pair of colliding atoms with the laser field through $\hat{H}_I(t)$. From Eqs. (2) and (3), the thermally averaged photoassociation probability into state $|\phi_\nu\rangle$ becomes

$$P_\nu(t)=\frac{1}{Z}\int_0^\infty e^{-\beta E}|\langle\phi_\nu|\hat{U}(t,0)|\phi(E)\rangle|^2dE, \tag{4}$$

where $\langle\phi_\nu|\hat{U}(t,0)|\phi(E)\rangle$ is the transition amplitude from the continuum state $|\phi(E)\rangle$ to the vibrational state $|\phi_\nu\rangle$ at time t. The total photoassociation probability is the summation of P_ν for all bound states $\Sigma_\nu P_\nu$. The following section presents a practical one-dimensional model to compute the photoassociation probability.

A. The binary collision model

A colliding pair of atoms is modeled as interacting through a Morse potential. In practice, the Morse potential is truncated at a long-range location L by an infinite barrier. The presence of the infinite barrier leads to discretization of the free Morse eigenstates and allows for treatment of the collision with square-integrable basis functions [25]. The field-free Hamiltonian for the relative motion is

$$H_0(x)=-\frac{\hbar^2}{2m_r}\frac{d^2}{dx^2}+V(x), \tag{5}$$

where m_r is the reduced mass of the colliding atoms and $V(x)$ is the truncated Morse potential,

$$V(x)=\begin{cases}V_M(x) & \text{for } x\leqslant L,\\ \infty & \text{otherwise.}\end{cases} \tag{6}$$

The Morse function is

$$V_M(x)=D(e^{-2\alpha(x-x_e)}-2e^{-\alpha(x-x_e)}), \tag{7}$$

where D is the well depth at the equilibrium position x_e, and α^{-1} is the potential range. The position of the barrier L is located sufficiently far outside the influence of the Morse oscillator, i.e., $L\gg\alpha^{-1}+x_e$ and $V_M(x=L)\approx 0$. There are two types of solutions for the eigenvalue equation of the field-free Hamiltonian in Eq. (5): bound eigenfunctions with negative energies $-D<E_\nu<0$ and unbound or scattering eigenfunctions with positive energies $E_m>0$. The bound eigenfunctions ϕ_ν are normalized as $\langle\phi_\nu|\phi_{\nu'}\rangle=\delta_{\nu\nu'}$ and obey the discretization rule

$$N_b-\sqrt{|\epsilon_\nu|}=\nu, \tag{8}$$

where ϵ_ν is the rescaled bound energy $\epsilon_\nu=2m_rE_\nu/(\hbar^2\alpha^2)$ and ν is a non-negative integer, which runs from 0 to the integer part of N_b and can be determined by the relation $2N_b+1=(8m_rD)^{1/2}/(\hbar\alpha)$. The unbound eigenfunctions $\phi_L(E_m)$ are normalized as $\langle\phi_L(E_m)|\phi_L(E_{m'})\rangle=\delta_{mm'}$ and follow the discretization condition (see Ref. [25] for details)

$$\alpha k_m(L-x_e)+\theta(k_m)=m\pi, \tag{9}$$

where the dimensionless rescaled momentum is $k_m=(2m_rE_m)^{1/2}/(\hbar\alpha)$ and $m=1,2,\ldots$. The phase shift $\theta(k_m)$ can be determined via the relation

$$\theta(k_m)=\arg\left(\frac{\Gamma(1+2ik_m)(2N_b+1)^{-ik_m}}{\Gamma(-N_b+ik_m)}\right), \tag{10}$$

where $\Gamma(z)$ is the Gamma function of complex argument. The time-dependent interaction Hamiltonian in the semiclassical dipole formulation is

$$H_I(x,t)=-\mu(x)\mathcal{E}(t), \tag{11}$$

where the dipole function is set to $\mu(x)=qxe^{-x/x_d}$, with q and x_d being constants, and the laser pulse $\mathcal{E}(t)$ starts at $t=0$ and ends at $t=t_f$. The matrix elements of the dipole function $\mu(x)$ with respect to the Morse eigenstate basis can be readily expressed analytically [31].

The discretization of the unbound states reduces the density operator $\hat{\rho}(t=0)$, Eq. (2), to the summation

$$\hat{\rho}_L(t=0)=\frac{1}{Z_L}\sum_{m=1}^{\infty}e^{-\beta E_m}|\phi_L(E_m)\rangle\langle\phi_L(E_m)|, \tag{12}$$

where the L-dependent partition function Z_L is

$$Z_L=\sum_{m=1}^{\infty}e^{-\beta E_m}. \tag{13}$$

The photoassociation probability into the bound state $|\phi_\nu\rangle$ at $t=t_f$, Eq. (4), becomes

$$P_{\nu,L}(t_f) = \frac{1}{Z_L}\sum_{m=1}^{\infty} e^{-\beta E_m} T_{\nu,L}(E_m). \tag{14}$$

The unbound→bound transition probabilities are

$$T_{\nu,L}(E_m) = |\langle \phi_\nu | \hat{U}_L(t_f,0) | \phi_L(E_m)\rangle|^2, \tag{15}$$

where the time-evolution operator $\hat{U}_L(t_f,0)$ depends on the location of the infinite barrier at L. The state-to-state transition probability, $T_{\nu,L}(E_m)$, can be obtained by solving the corresponding time-dependent Schrödinger equation. The total photoassociation probability is the sum of $P_{\nu,L}(t_f)$ over all bound states

$$P_L(t_f) = \sum_{\nu=0}^{\mathrm{Int}[N_b]} P_{\nu,L}(t_f), \tag{16}$$

where $\mathrm{Int}[N_b]$ is the integer part of N_b.

In the limit $L\to\infty$, Eq. (14) can be recast as

$$\lim_{L\to\infty} Z_L P_{\nu,L}(t_f) = \lim_{L\to\infty} \int_0^{\infty} e^{-\beta E_m} \frac{dm}{dE_m} \times |\langle \phi_\nu | \hat{U}(t_f,0) | \phi_L(E_m)\rangle|^2 dE_m, \tag{17}$$

where the density of states dm/dE_m can be obtained from the discretization condition (9),

$$\frac{dm}{dE} = \frac{1}{\alpha\pi\hbar}\sqrt{\frac{m_r}{2E}}\left(\alpha(L-x_e) + \frac{d\theta(k)}{dk}\right), \tag{18}$$

and the unbound eigenstates satisfy the relation [25,31]

$$\lim_{L\to\infty} \sqrt{\frac{dm}{dE_m}} |\phi_L(E_m)\rangle = |\phi(E_m)\rangle. \tag{19}$$

Substitution of Eqs. (18) and (19) into Eq. (17) yields the non-normalized photoassociation probability from the continuum,

$$\lim_{L\to\infty} Z_L P_{\nu,L}(t_f) = \int_0^{\infty} e^{-\beta E} |\langle \nu | \hat{U}(t_f,0) | \phi(E)\rangle|^2 dE = Z P_\nu(t_f), \tag{20}$$

where $|\phi(E)\rangle$ refers to the Morse continuum eigenstates, satisfying the orthogonality relation $\langle\phi(E)|\phi(E')\rangle = \delta(E-E')$. In the limit $L\to\infty$, the partition function Z_L becomes

$$\lim_{L\to\infty} Z_L = \int_0^{\infty} e^{-\beta E_m} \frac{dm}{dE_m} dE_m \approx \frac{L}{2\pi\hbar}\sqrt{\frac{2\pi m_r}{\beta}}, \tag{21}$$

which gives rise to the L dependence of $P_{\nu,L}(t_f)$.

In setting a value for the position of the infinite barrier, the collision of each atomic pair can be regarded as taking place within a relative distance L. Since a one-dimensional model is considered, the photoassociation probability for the system can be regarded to scale with density as L^{-1} [23]. In practice, the value of L is chosen to be sufficiently large such that convergence occurs with no significant change of the non-normalized photoassociation probability. In this case, Eqs. (20) and (21) show that the probabilities for still larger values of L, or equivalently lower densities, are determined by the converged probability apart from a scaling factor. Therefore, in a situation where Eq. (20) is numerically converged, $P_{\nu,L}$ already incorporates all the relevant physics associated with the photoassociation transition probability. For instance, given two distinct converged values for the barrier position L_1 and L_2, the corresponding transition probabilities are related by $P_{\nu,L_1} = (Z_{L_2}/Z_{L_1}) P_{\nu,L_2}$.

B. Photoassociation upper bound

For a general controllable N-level quantum system, it is possible to derive the maximum attainable expectation value of an Hermitian observable operator $\hat{O}(t_f)$ [26–30]. The full controllability of the system implies that any mixed quantum state $\hat{\rho}(t_f)$ in the same kinematic equivalence class [27] as the initial one $\hat{\rho}(t=0)$ can be reached dynamically. The observable $\hat{O}(t_f)$ and the initial density matrix $\hat{\rho}(t=0)$ may be expressed in diagonal form and their respective eigenvalues may be ordered as $\Lambda_1^O \geqslant \Lambda_2^O \geqslant \cdots \geqslant \Lambda_N^O$ and $\Lambda_1^\rho \geqslant \Lambda_2^\rho \geqslant \cdots \geqslant \Lambda_N^\rho$. It follows that the expectation value of $\hat{O}(t_f)$ has an upper bound given by [26]

$$\langle \hat{O}(t_f)\rangle = \mathrm{Tr}[\hat{O}\hat{U}(t_f,0)\hat{\rho}(t=0)\hat{U}^\dagger(t_f,0)] \leqslant \sum_{i=1}^{N} \Lambda_i^O \Lambda_i^\rho. \tag{22}$$

The operator of concern here is the projection operator onto all bound states $\hat{O}(t_f) = \Sigma_\nu |\phi_\nu\rangle\langle\phi_\nu|$. Thus, it is possible to readily determine from Eqs. (16) and (22) the maximum possible photoassociation yield $Q_L(T)$ at a temperature T,

$$Q_L(T) = \frac{1}{Z_L}\sum_{m=1}^{\mathrm{int}(N_b+1)} \exp(-\beta E_m). \tag{23}$$

Furthermore, in the limit of large L the energies E_m in the above summand tend to approach zero and $Q_L Z_L$ approaches the number of bound states, $\mathrm{int}(N_b+1)$. Then, from Eqs. (20) and (23) the maximum possible photoassociation yield in the continuum case $Q(T)$ is related to the case with the barrier by

$$ZQ(T) = \lim_{L\to\infty} Z_L Q_L(T) = \mathrm{Int}(N_b+1). \tag{24}$$

Thus, the upper limit to the photoassociation probability is proportional to the number of bound states of the molecule to be formed. Although the calculation leading to Eq. (24) was carried out for the specific model system considered here, this result is far more general. For instance, taking into account rotational degrees of freedom and the possibility of electronic excitation, one can conclude following the same line of reasoning that the upper bound of the photoassociation probability is still proportional to the corresponding number of bound states. The analysis leading to Eqs. (23) and (24) does not identify an optimal field leading to this maximum possible control result. However, $Q_L(T)$ provides an upper limit to compare with using *a priori* chosen fields and a target goal for subsequent optimal control studies.

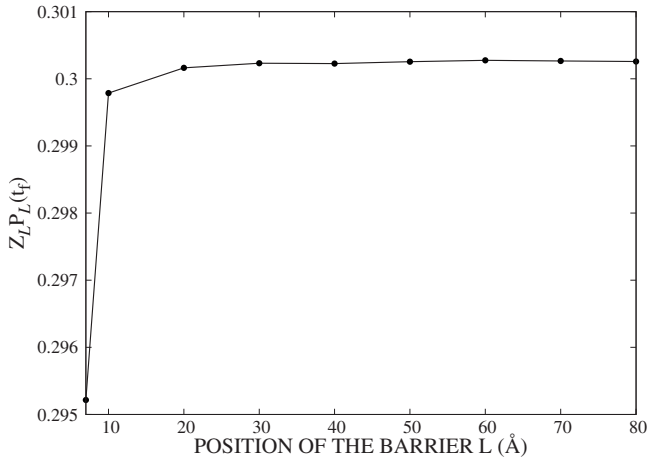

FIG. 1. Non-normalized total photoassociation probability $Z_L P_L(t_f)$ as a function of the barrier position L. The field parameters are amplitude $V_0=100$ MV cm^{-1}, frequency $\omega=0.028$ eV, and duration $t_f=0.5$ ps. The temperature is $T=100$ K.

III. RESULTS AND DISCUSSIONS

The binary collision model described in the previous section is illustrated numerically for the photoassociation reaction

$$\mathrm{O} + \mathrm{H} \underset{\mathcal{E}(t)}{\longrightarrow} \mathrm{OH}, \tag{25}$$

where the electric field assumes a simple sine-squared pulse form

$$\mathcal{E}(t) = \begin{cases} V_0 \sin(\pi t/t_f)^2 \cos(\omega t) & \text{for } 0 \leqslant t \leqslant t_f, \\ 0 & \text{otherwise}, \end{cases} \tag{26}$$

with amplitude V_0 and carrier frequency ω. The Morse parameters in Eq. (7) are $D=5.4$ eV, $\alpha^{-1}=0.445$ Å, $x_e=0.9639$ Å, and the reduced mass of OH is $m_r=0.9482$ u. There are 22 bound states supported by the Morse potential, noting that $N_b \approx 21.58$ from Eq. (8). The parameters of the dipole function are $q=1.634|e|$ and $x_d=0.6$ Å in Eq. (11). Temperatures up to $T=500$ K are considered, for which $k_B T=0.043$ eV. A typical value for the field bandwidth used here is 0.014 eV, corresponding to a pulse duration of $t_f=0.5$ ps. For a peak amplitude of $V_0=50$ MV cm^{-1} and $x=x_e$, the coupling strength is roughly 0.4 eV.

Figure 1 shows the non-normalized probability $Z_L P_L(t_f)$ as a function of the position of the infinite barrier L for $T=100$ K, $V_0=100$ MV cm^{-1}, $\omega=0.028$ eV, and $t_f=0.5$ ps. It is seen that for $L>20$ Å the non-normalized photoassociation probability is essentially constant. The barrier position at $L=50$ Å proved to be sufficiently large to guarantee the convergence of $Z_L P_{v,L}(t_f)$ for all parameter values used in this work. However, it should be noted that other choices for the external field may, in general, require different values for the barrier position in order to guarantee reasonable satisfaction of Eq. (20).

Figure 2 shows the thermal probability density $\langle x|\hat{\rho}_L(t)|x\rangle$ as a function of x at $t=0$ and $t=t_f$, using the same parameters of Fig. 1 and the barrier set at $L=50$ Å. At $t=0$, the thermal density is oscillatory around the equilibrium position of the

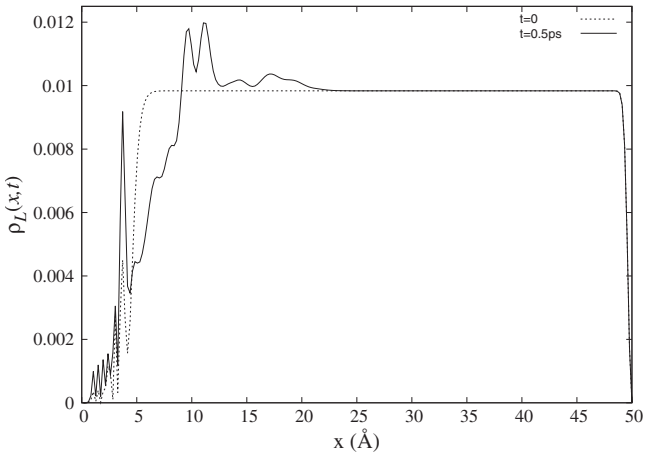

FIG. 2. Thermal probability density $\rho_L(x,t)=\langle x|\hat{\rho}_L(t)|x\rangle$ for $t=0$ and 0.5 ps for the same parameters of Fig. 1 and for $L=50$ Å.

Morse well, becomes constant beyond $x=5$ Å, and approaches zero at $x=50$ Å because of the infinite barrier. At $t=t_f$, the increase of the thermal density in the Morse potential well region ($x<5$ Å) is related to transitions into the bound states, as analyzed below. There is also an increase of the thermal density between 9 and 22 Å relative to that at $t=0$ due to the presence of transitions amongst the unbound states. The fact that the thermal density remains unchanged for $x \geqslant 22$ Å throughout the pulse duration $t \in [0, t_f]$ indicates convergence of the calculations for a choice of $L \geqslant 22$ Å, which is consistent with the convergence shown in Fig. 1.

The maximum photoassociation yield $Q_L(T)$ in Eq. (23) for $L=4000$ Å as a function of the temperature is depicted in Fig. 3. $Q_L(T)$ decreases as T increases due to involvement of more unbound states in the partition function at higher temperatures. At low temperatures, higher yields are possible because a small number of unbound states are involved. The maximum yield for $T=1$ K is about 0.1 and for $T=500$ K it

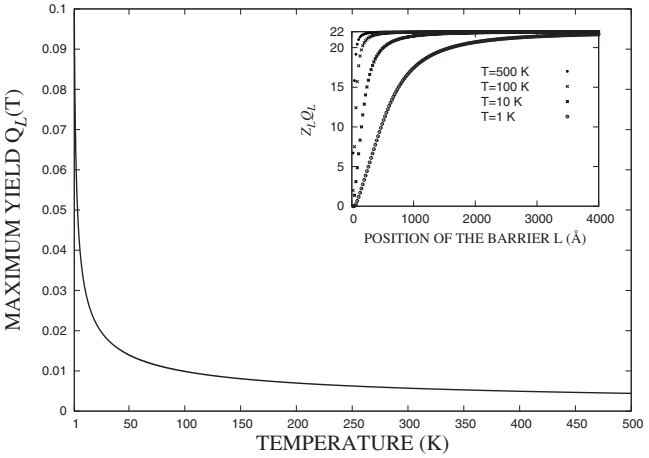

FIG. 3. Maximum possible photoassociation yield as a function of the temperature for $L=4000$ Å. At any temperature T an optimal field would need to be sought in order to reach the value $Q_L(T)$. The inset shows the convergence of the non-normalized maximum yield to the number of molecular bound states.

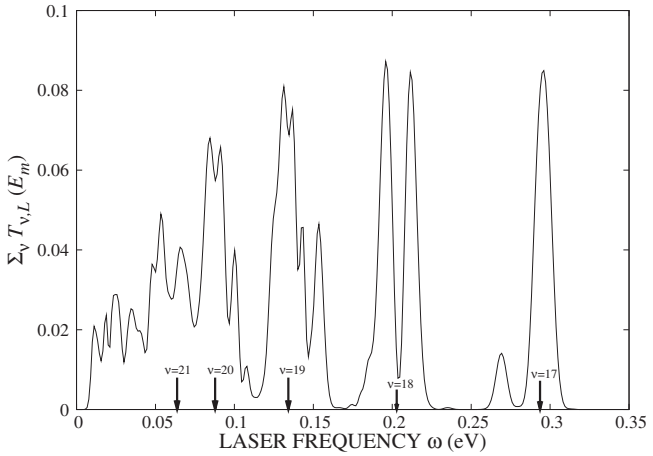

FIG. 4. Transition probability to all of the bound states from a single scattering state with energy E_m=0.06 eV as a function of the carrier laser frequency. The external field parameters are V_0 =100 MV cm^{-1}, t_f=0.5 ps. The arrows indicate the frequencies that match the single-photon resonance condition to excited bound levels. The barrier position is L=50 Å.

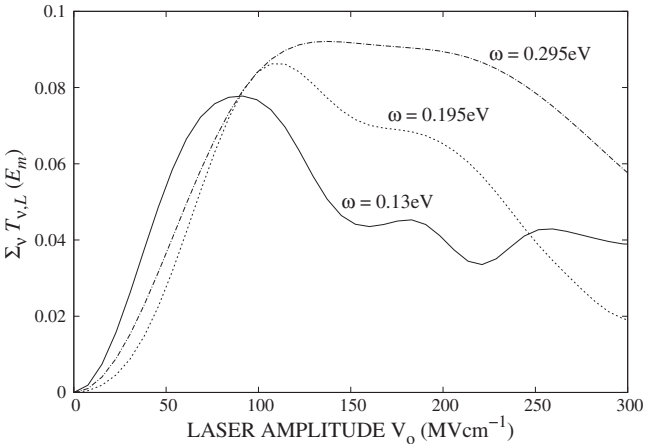

FIG. 5. Transition probability to all of the bound states from a single scattering state with energy E_m=0.06 eV as a function of the laser peak amplitude for three labeled laser frequencies. The pulse duration is t_f=0.5 ps and the barrier position is L=50 Å.

is 0.005. The inset shows the convergence of the non-normalized maximum yield $Z_L Q_L(T)$ for several temperatures. The non-normalized maximum yield approaches the total number of bound states of the molecule. The value of L for the convergence of the maximum yield is much larger than the converged L value for the transition probabilities calculated for the fixed-shape pulses used here. This is related to the fact that Eq. (23) involves only the unbound energies and the temperature, whereas Eq. (16) crucially depends on the nature of the laser field.

A. Single-scattering-state photoassociation

First consider photoassociation starting from a single unbound state $|\phi_L(E_m)\rangle$ setting the barrier position to L=50 Å. This preliminary step can reveal the detailed structure of the state-to-state photoassociation processes to aid in judiciously choosing the parameters of the laser pulse. Since this is a pure-state case, the upper bound for the transition probability is 1 [26]. Figure 4 shows the unbound→bound transition probability of Eq. (15) summed over all bound states $\Sigma_\nu T_{\nu,L}(E_m)$ as a function of the laser carrier frequency. The transition probability is calculated at $t=t_f$ and the initial unbound state has energy E_m=0.06 eV, which corresponds to the scattering level m=78. This initial state energy is chosen in the region of the maximum bound-unbound matrix element $\langle\phi_\nu|\mu|\phi_L(E_m)\rangle$ and also corresponds to the mean wave packet energy used in Ref. [18]. The pulse duration is t_f =0.5 ps and the amplitude is V_0=100 MV cm^{-1}. The observed peaks arise from single- and multiphoton transitions between the initial scattering state and the bound states. The n-photon resonance condition is given by $n\omega=(E_m-E_\nu)/\hbar$, although precise correlation with the peak in Fig. 4 can be influenced by the dynamical power shifting of the energy levels due to the strong field. Some single-photon transitions to the bound levels are indicated by arrows in the figure. For low frequencies (<0.1 eV), the transitions occur to the highest excited levels, which are closely spaced, especially to the ν=21,20 states, respectively at 0.0037 and 0.0278 eV below the dissociation limit. For higher frequencies, the peaks are related to single-photon transitions to the ν=19,18,17 states, respectively at 0.0742, 0.1428, 0.2336 eV below the dissociation threshold. Concurrently with the more evident single-photon transitions, there also exists multiphoton transitions. For instance, the peak at ω=0.29 eV occurs due to a single-photon transition into the ν=17 state (reaching a final population of 0.076) and also to three-photon transition to the ν =13 state (reaching a population of 0.008). Finally, we note that population below the ν=11 state is negligible. This can be understood in view of the bound-unbound matrix elements [31], which have very small amplitude for the strongly bound levels $\nu<11$.

Figure 5 shows the overall continuum→bound transition probability $\Sigma_\nu T_{\nu,L}(E_m)$ as a function of the external pulse amplitude for three frequencies: ω=0.13, ω=0.195, and ω =0.295 eV. These frequencies were chosen to coincide with some of the peaks in Fig. 4. The highest probabilities of the three curves are found for the field amplitude in the range from 50 to 200 MV cm^{-1}. The transition probabilities in Figs. 4 and 5 are very low compared to unity, which is the maximum attainable probability in this case. As shown in the next section, the thermal average probability obtained for the subpicosecond pulses given in Eq. (26) is also well below the photoassociation upper bound.

Before examining the thermal-averaged calculations, consider the Boltzmann-weighted transition probability $T_{B,L}(E_m)$ for a single scattering state $|\phi_L(E_m)\rangle$ defined by

$$T_{B,L}(E_m) = \frac{e^{-\beta E_m}}{Z_L} \sum_{\nu=0}^{\mathrm{int}(N)} T_{\nu,L}(E_m). \tag{27}$$

Figure 6 presents the Boltzmann-weighted transition probability as a function of the initial scattering-state energy for T=100 and 500 K. The external field parameters are ω =0.147 eV, V_0=50 MV cm^{-1}, and t_f=0.5 ps. For comparison, the inset shows the transition probability summed over

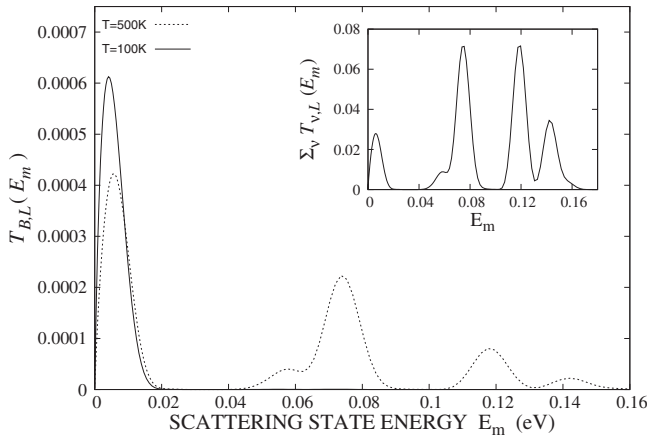

FIG. 6. Boltzmann-weighted transition probability into all of the bound states in Eq. (27) as a function of the initial scattering-state energy for $T=500$ and 100 K. The external field duration $t_f=0.5$ ps with frequency $\omega=0.147$ eV and amplitude $V_0=40$ MV cm^{-1}. The inset shows the transition probability summed over the bound states without the Boltzmann factor. The barrier position is $L=50$ Å.

all bound states without the Boltzmann factor $\Sigma_\nu T_{\nu,L}(E_m)$. It is evident that the transitions from high scattering energies are damped by the Boltzmann factor. It is also evident that the peak at low energy is comparatively higher for $T=100$ K than for $T=500$ K. The broadening of the Boltzmann distribution as the temperature increases allows for more transitions among scattering and bound states to be taken into account in the thermal average, however this is also accompanied by an increment of the partition function, as $Z_L \propto T^{1/2}$. Therefore, the trade-off between these factors will give the peak photoassociation yield at some particular temperature T for fixed laser-pulse parameters.

B. Thermal-averaged photoassociation

In this section, the probabilities are found with respect to a barrier position at $L=4000$ Å, allowing for comparison

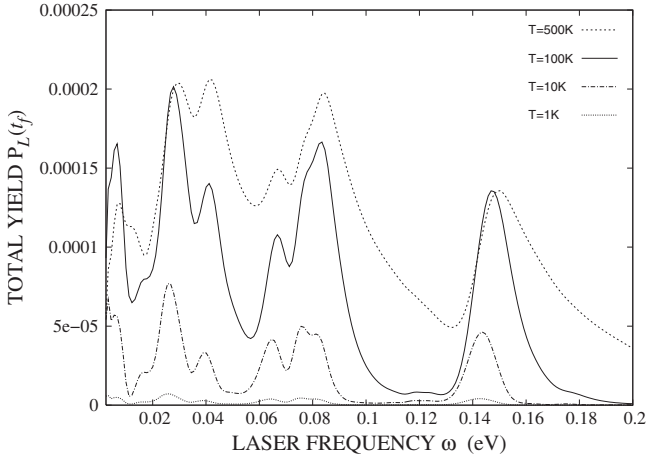

FIG. 7. Thermal-averaged photoassociation probability $P_L(t_f)$ into all of the bound states in Eq. (16) as a function of the field frequency ω. The external field has amplitude $V_0=50$ MV cm^{-1} and duration $t_f=0.5$ ps. The barrier position is $L=4000$ Å.

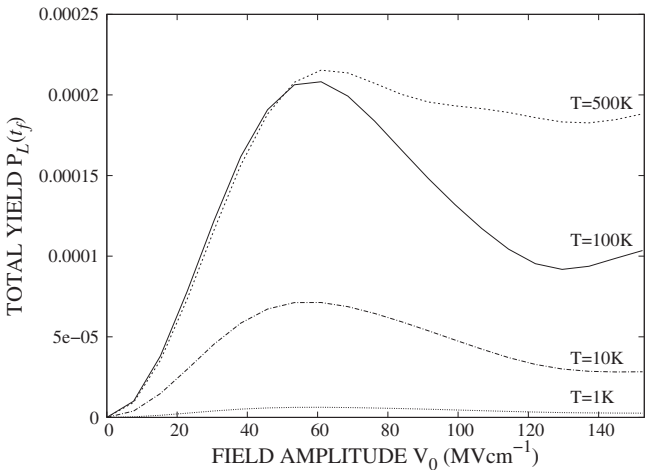

FIG. 8. Thermal-averaged photoassociation probability $P_L(t_f)$ into all of the bound states as a function of the field amplitude V_0 for several temperatures. The external field duration is $t_f=0.5$ ps and the frequency is $\omega=0.028$ eV. The barrier position is $L=4000$ Å.

with the maximum yield in Fig. 3 and corresponding to a system with linear density of the order of 10^4 atoms/cm. Figure 7 shows the total thermally averaged photoassociation probability $P_L(t_f)$, Eq. (16), as a function of the laser frequency ω at four temperatures $T=1$, 10, 100, 500 K, and for $V_0=50$ MV cm^{-1}, and $t_f=0.5$ ps. At least four major peaks are observed: the first below $\omega=0.01$ eV, and the others around 0.03, 0.08, and 0.147 eV. The total photoassociation probability increases as the temperature increases from 1 to 100 K. However, the total photoassociation probability decreases for $\omega<0.01$ eV and $\omega=0.147$ eV as the temperature rises from 100 to 500 K.

The total thermally averaged photoassociation probability $P_L(t_f)$ as a function of the laser amplitude V_0 is depicted in Fig. 8 for several temperatures calculated for the pulse frequency $\omega=0.028$ eV and for the pulse duration $t_f=0.5$ ps.

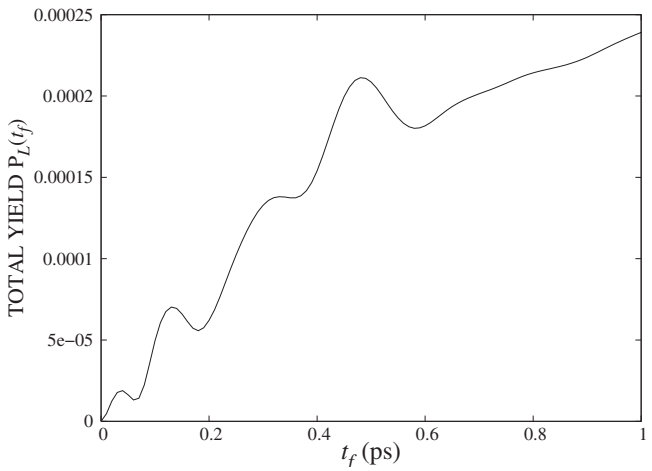

FIG. 9. Thermal-averaged photoassociation probability $P_L(t_f)$ into all of the bound states as a function of the duration of the external pulse t_f. The external field amplitude is $V_0=60$ MV cm^{-1} and the frequency is $\omega=0.028$ eV. The temperature is set to $T=100$ K. The barrier position is $L=4000$ Å.

The curves have maxima around $V_0=60$ MV cm^{-1}, and as in the case of Fig. 7, the total photoassociation probability increases with the temperature between 1 and 100 K. However, further raising of the temperature from 100 to 500 K leads to a decrease in the total photoassociation probability for pulse amplitudes below $V_0=70$ MV cm^{-1}. The temperature dependence observed in Figs. 7 and 8 may be understood as a trade-off between the Boltzmann factors and the partition function [cf. Eq. (14)].

Figure 9 shows the total photoassociation probability as a function of the duration of the pulse t_f, with $V_0=60$ MV cm^{-1}, $\omega=0.028$ eV, and $T=100$ K. There is oscillatory behavior along with an overall increase of the photoassociation probability as the pulse duration is increased. The total photoassociation yield for pulses below 1 ps remains very low compared to the optimal photoassociation probability of 0.01 of Fig. 3 at $T=100$ K. Figures 7–9 indicate that no simple adjustment of the parameters in the sine-squared pulse of Eq. (26) can approach the optimal yield depicted in Fig. 3. The probabilities obtained for the fixed-shape pulses were at least 20 times below the optimal value.

IV. CONCLUSION

This work investigated the formation of diatomic molecules induced by an external laser pulse in a thermal gas of atoms. A nonperturbative treatment was presented based on a simple one-dimensional model for the atomic binary collisions. In the context of quantum optimal control theory, assuming full system controllability, we determined the maximum possible photoassociation yield which could be produced by an appropriate optimally designed field. It was shown that the maximum yield is proportional to the number of bound states of the molecule being formed. This result is not restricted to the model considered here and is valid in more general situations when rotation and electronic excitation are taken in account. In the numerical calculations, the total photoassociation probability was found to have a complex dependence on the parameters for a fixed-shape pulse and the temperature. Single-photon- and multiphoton-driven transitions are involved in the photoassociation dynamics. However, the photoassociation yield was more than one order of magnitude lower than the upper bound for any choice of the pulse parameters. The formulation and results of this paper lay the groundwork for proceeding with full optimal control calculations to determine the nature of the fields that can reach the maximum attainable yield.

ACKNOWLEDGMENTS

The authors acknowledge support from CAPES-Brazil and the U.S. Department of Energy.

[1] H. Rabitz, R. de Vivie-Riedle, M. Motzkus, and K. Kompa, Science **288**, 824 (2000).
[2] K. M. Jones, E. Tiesinga, P. D. Lett, and P. S. Julienne, Rev. Mod. Phys. **78**, 483 (2006).
[3] R. A. Cline, J. D. Miller, and D. J. Heinzen, Phys. Rev. Lett. **73**, 632 (1994).
[4] J. H. Schloss, R. B. Jones, and J. G. Eden, Chem. Phys. Lett. **191**, 195 (1992).
[5] E. B. Gordon, V. G. Egorov, S. E. Nalivaiko, V. S. Pavlenko, and O. S. Rzhevsky, Chem. Phys. Lett. **242**, 75 (1995).
[6] G. Inoue, J. K. Ku, and D. W. Setser, J. Chem. Phys. **76**, 733 (1982).
[7] A. H. Zewail, J. Phys. Chem. A **104**, 5660 (2000).
[8] E. D. Potter, J. L. Herek, S. Pedersen, Q. Liu, and A. H. Zewail, Nature (London) **355**, 66 (1992).
[9] U. Marvet and M. Dantus, Chem. Phys. Lett. **245**, 393 (1995).
[10] J. Weiner, V. S. Bagnato, S. Zilio, and P. S. Julienne, Rev. Mod. Phys. **71**, 1 (1999).
[11] M. Kostrun, M. Mackie, R. Cote, and J. Javanainen, Phys. Rev. A **62**, 063616 (2000).
[12] J. M. Hutson and P. Soldan, Int. Rev. Phys. Chem. **25**, 497 (2006).
[13] W. Salzmann *et al.*, Phys. Rev. A **73**, 023414 (2006).
[14] C. P. Koch, R. Kosloff, and F. Masnou-Seeuws, Phys. Rev. A **73**, 043409 (2006).
[15] A. Fioretti, D. Comparat, A. Crubellier, O. Dulieu, F. Masnou-Seeuws, and P. Pillet, Phys. Rev. Lett. **80**, 4402 (1998).
[16] A. Vardi, D. Abrashkevich, E. Frishman, and M. Shapiro, J. Chem. Phys. **107**, 6166 (1997).
[17] M. V. Korolkov, J. Manz, G. K. Paramonov, and B. Schmidt, Chem. Phys. Lett. **260**, 604 (1996).
[18] E. F. de Lima and J. E. M. Hornos, Chem. Phys. Lett. **433**, 48 (2006).
[19] P. Marquetand and V. Engel, J. Chem. Phys. **127**, 084115 (2007).
[20] Y.-Y. Niu, S.-M. Wang, and S.-L. Cong, Chem. Phys. Lett. **428**, 7 (2006).
[21] M. V. Korolkov and B. Schmidt, Chem. Phys. Lett. **272**, 96 (1997).
[22] E. J. Heller and H. A. Yamani, Phys. Rev. A **9**, 1201 (1974).
[23] C. P. Koch, R. Kosloff, E. Luc-Koenig, F. Masnou-Seeuws, and A. Crubellier, J. Phys. B **39**, S1017 (2006).
[24] M. Mackie and J. Javanainen, Phys. Rev. A **60**, 3174 (1999).
[25] E. F. de Lima, T.-S. Ho, and H. Rabitz, J. Phys. A **41**, 335303 (2008).
[26] T.-S. Ho and H. Rabitz, J. Photochem. Photobiol., A **180**, 226 (2006).
[27] S. G. Schirmer, A. I. Solomon, and J. V. Leahy, J. Phys. A **35**, 4125 (2002).
[28] R. Chakrabarti and H. Rabitz, Int. Rev. Phys. Chem. **26**, 671 (2007).
[29] H. Rabitz, T.-S. Ho, M. Hsieh, R. Kosut, and M. Demiralp, Phys. Rev. A **74**, 012721 (2006).
[30] S. Shi and H. Rabitz, J. Chem. Phys. **92**, 364 (1990).
[31] E. F. de Lima and J. E. M. Hornos, J. Chem. Phys. **125**, 164110 (2006).